Astragaloside IV inhibits excessive mesangial cell proliferation and renal fibrosis caused by diabetic nephropathy via modulation of the TGF-β1/Smad/miR-192 signaling pathway

QIAN MAO[1], CUICUI CHEN[2], HUANKUN LIANG[2], SHUHAI ZHONG[2], XINBO CHENG[3] and LAIQING LI[2]

[1]Department Endocrinology, Hospital of Beihua University, Jilin, Jilin 132013;
[2]Guangzhou Youdi Bio-Technology Co., Ltd., Guangzhou, Guangdong 510663;
[3]Department of Endocrinology and Metabolism, Hospital of Soochow University, Suzhou, Jiangsu 210506, P.R. China

Received December 13, 2018; Accepted July 12, 2019

DOI: 10.3892/etm.2019.7887

Abstract. Astragaloside IV (ASI) exhibits a wide variety of pharmacological effects in cardiovascular diseases, hepatitis and kidney disease and due to this, ASI has recently become an attractive research target. The present study aimed to determine the effect of ASI on renal fibrosis and the mechanisms underlying its therapeutic effects in diabetic nephropathy (DN). *In vitro*, ASI was added to rat mesangial cells (RMCs) and cultured with a high level of glucose (HG) to observe the effects exhibited on proliferation and fibrosis-related mRNA and protein expression. *In vivo*, a DN model was established using streptozotocin administration in rats, and renal injury was evaluated using renal histological examination. The expression levels of related mRNAs and proteins were analyzed using reverse transcription-quantitative PCR, western blot analysis and immunohistochemistry. ASI was demonstrated to downregulate miR-192 expression and inhibit excessive proliferation of RMCs, which was induced by HG, in a dose-dependent manner. Additionally, ASI exhibited a therapeutic effect on DN rats. ASI was also demonstrated to decrease the miR-192 expression and mRNA and protein expression of transforming growth factor-β1 (TGF-β1), Smad3, α-smooth muscle actin (α-SMA) and collagen type 1 (col1), and increase the mRNA and protein expression of Smad7 *in vitro* and *in vivo*. These results suggested that ASI exhibited a therapeutic effect on DN, possibly due to the inhibition of excessive mesangial proliferation and renal fibrosis via the TGF-β1/Smad/miR-192 signaling pathway.

Correspondence to: Mr. Laiqing Li, Guangzhou Youdi Bio-Technology Co., Ltd., 3 Juquan Road, Guangzhou, Guangdong 510663, P.R. China
E-mail: lilaiqing191@163.com

Key words: astragaloside IV, diabetic nephropathy, transforming growth factor-β1/Smad/microRNA-192 pathway, proliferation, renal fibrosis

Introduction

The number of individuals with diabetes is rapidly increasing every year and by 2030, disease prevalence is expected to reach 4.4%, with >366 million patients suffering from this disease (1). Diabetes is a severe disorder that increases the risk of microvascular complications. The kidney is one of the main organs affected by microvascular injury, and this makes diabetic nephropathy (DN) one of the most common complications exhibited by patients with diabetes (2,3). DN is the most common single cause of end-stage renal failure and affects 40-45% of patients entering renal replacement therapy programs (4). The main renal histological changes that are typical of DN are caused by the excessive deposition of extracellular matrix (ECM). ECM accumulation results in glomerular sclerosis and tubulointerstitial fibrosis and, eventually, a large proportion of patients exhibiting ECM develop chronic renal failure (5,6). The effect of the transforming growth factor-β1 (TGF-β1)/Smad3 signaling pathway on the mediation of renal fibrosis has been well recognized, and the inhibition of the TGF-β1/Smad3 signaling pathway has been revealed to be an effective approach in preventing DN progression (7,8).

In the Chinese Pharmacopoeia, herbal drug Radix Astragali Mongolici is described as the dried root of the Mongolian leguminous *Astragalus* plants (9). The constituents of Radix Astragali Mongolici include saponins, polysaccharides and flavonoids, and >40 constituents have been identified in the *Astragalus* root (10,11). Astragalosides, the major active components of Radix Astragali Mongolici, consist of numerous triterpene saponins, including astragalosides I-IV (12). Astragaloside IV (ASI) is the major active constituent of *Astragalus membranaceus* (also known as huangqi) and has been widely used for the treatment of cardiovascular diseases, hepatitis, kidney disease and skin diseases in China (13,14). The hepatoprotective and antifibrotic effects of ASI have been supported in previous studies (15,16). Despite the increase in the clinical usage of ASI, the mechanisms underlying its therapeutic effects on DN remain not clearly understood and require further investigation.

Based on the results of previous studies, it can be hypothesized that the therapeutic and antifibrotic effects of

ASI on DN are associated with the TGF-β1/Smad signaling pathway (13-16). Therefore, the current study established a rat mesangial cell (RMC) model, induced by high glucose (HG), and a DN rat model to assess this. Cells were cultured in different ASI doses and rats were administered ASI via gavage, to determine the underlying mechanisms of the therapeutic effects of ASI in DN.

Materials and methods

Animals, cells and reagents. A total of 24 adult Sprague-Dawley (SD) rats (male/female 1:1, age, 9 weeks; weight, 200-220 g) were purchased from the Animal Research Center of Southern Medical University. The rats were housed in an Specific pathogen Free (SPF)-grade laboratory with a temperature-controlled of (25˚C±2˚C) and a 12-h light/dark cycle with free access to food and water. All efforts were made to minimize animal suffering and reduce the number of animals used. Rat mesangial cells (RMCs; cat. no. CRL-2573) were obtained from the American Type Culture Collection. The cells were cultured in DMEM (Gibco; Thermo Fisher Scientific, Inc.) supplemented with 10% FBS (Gibco; Thermo Fisher Scientific, Inc.) at 37˚C in a 5% CO_2 humidified atmosphere. ASI was purchased from Shanghai Jizhi Biochemical Technology Co., Ltd. (cat. no. A50670; purity ≥99%, as determined by the manufacturer; HPLC).

In vitro experiment. Near-confluent (80% confluent) RMCs were incubated with DMEM supplemented with 2% FBS at 37˚C for 24 h, to arrest and synchronize cell growth, synchronized RMCs were cultured at 37˚C in normal DMEM with 5.5 nM glucose (low-glucose, LG; Sigma-Aldrich; Merck KGaA; cat. no. G8270) or 30 nM glucose (high-glucose, HG) for 72 h, and RMCs were then collected for reverse transcription-quantitative (RT-q) PCR assay. The synchronized RMCs were co-cultured at 37˚C in the presence of HG and ASI (0, 10, 20, 50, and 100 μg/ml) for 72 h and subsequently used for the assessment of miR-192 expression and cell proliferation. RMCs cultured with LG, HG, and a combination of HG and 50 μg/ml ASI for 72 h, were used in the western blot analysis.

RNA extraction and RT-qPCR. Total RNA was extracted from RMCs using TRIzol reagent (Thermo Fisher Scientific, Inc.), and a cDNA Synthesis kit (Takara Biotechnology Co., Ltd.) was subsequently used to synthesize cDNA. RT-qPCR was performed to assess microRNA (miRNA) and mRNA expression using a LightCycler 480 detection system (Roche Diagnostics) and SYBR Green dye (cat. no. S7567; Invitrogen; Thermo Fisher Scientific, Inc.). cDNA reverse transcription (RT) was performed using a Reverse Transcriptase kit (cat. no. D2639A; Takara Biotechnology Co., Ltd.) at 37˚C for 15 min. The thermocycling conditions were as follows: Initial denaturation at 92˚C for 4 min, followed by 40 cycles of 90˚C for 15 sec and 60˚C for 30 sec. The primers used are listed in Table I. Primers were designed using Primer Express version 2.0 software (Applied Biosystems; Thermo Fisher Scientific, Inc.). The primer specificities were confirmed using The National Center for Biotechnology Information Primer-BLAST web tool (17). GAPDH mRNA and U6 small nuclear RNA levels were used for normalization. The RT-qPCR data were analyzed and expressed as relative miRNA or mRNA levels using cycle threshold values, which were subsequently converted to fold change values using the $2^{-\Delta\Delta Cq}$ method (18).

Cell proliferation assay. RMCs at 80% confluence were incubated with DMEM supplemented with 2% FBS 37˚C for 24 h, to arrest and synchronize cell growth. The synchronized RMCs were seeded in triplicate in 96-well plates ($1x10^3$ cells/well) and co-cultured at 37˚C in the presence of HG and ASI (0, 10, 20, 50, and 100 μg/ml) with DMEM supplemented with 10% FBS for 0, 24, 48 and 72 h respectively. After culture, 10 μl of Cell Counting kit-8 reagent (Beyotime Institute of Biotechnology) was added to the medium, and the cells were incubated for 1 h. Cell proliferation was assessed at 24, 48 and 72 h by measuring the absorbance at 450 nm using a microplate reader (680 Microplate Reader; Bio-Rad Laboratories, Inc.). Assays were repeated three times.

In vivo experiment. After one week of adaptation, diabetes was induced via a single intraperitoneal injection of streptozotocin (Sigma-Aldrich; Merck KGaA) diluted in citrate buffer (0.1 mol/l; pH 4.0) at a dose of 45 mg/kg (19). The sham group (6 rats) were intraperitoneally injected with an equal volume of 0.1 mol/l citrate buffer without streptozotocin. The rats were then fed a normal diet for an additional three weeks; during this time, blood glucose was maintained at >16.7 mmol/l, the 24 h urine output was >150% above normal levels and urinary protein excretion was >30 mg/24 h, which indicated the successful establishment of the DN rat model (6). Six rats failed to meet the above requirements and were eliminated from the current study. The model rats were randomly divided into two groups: The model group and the model + ASI group, with 6 rats in each. The model + ASI group rats were subjected to daily intragastric administration of 40 mg/kg ASI for 8 weeks, and the sham group and model group rats were orally administered 40 mg/kg saline for 8 weeks. The diet, exercise and mental state (assessed via visual inspection of behaviors including depression and hyperactivity) of all rats were monitored daily. After 8 weeks of treatment, urine was collected and after weighing, rats were euthanized, and blood samples were collected via cardiac puncture. The kidney tissue was immediately isolated, weighed and frozen at -80˚C for subsequent use in western blot analysis, RT-qPCR, histological examination and immunohistochemistry.

Biochemical analysis. The levels of urine protein were determined using a urinary protein kit (cat. no. C035-2; Nanjing Jiancheng Bioengineering Institute). Creatinine and blood urea nitrogen levels were determined using a creatinine assay kit (cat. no. C011-2; Nanjing Jiancheng Bioengineering Institute) and a urea assay kit (cat. no. C013-2; Nanjing Jiancheng Bioengineering Institute).

Western blot analysis. Collected kidney tissues or RMCs were lysed in radioimmunoprecipitation assay buffer (Roche Diagnostics) using manufacturer's protocol. Protein concentration was measured using the Micro BCA protein assay kit (Youdi Bio-technology Co., Ltd, China). Total proteins (50 μg) were loaded into each lane and 12% SDS-PAGE was

Table I. Primer sequences.

Primer name	Primer sequence (5'-3')	
	Forward	Reverse
H-miR-192	RT primer: CUGACCUAUGAAUUGACAGCCGTCGTATCCAGTGCGTGTCGTGGAGT CGGCAATTGCACTGGATACGACGGCTGTCA	
	GGGCTGACCTATGAATTG	CAGTGCGTGTCGTGGAGT
H-U6	RT primer: GTCGTATCCAGTGCAGGGTCCGAGGTATTCGCACTGGATACGACAAA AAT	
	ACGATGCACCTGTACGATCA	TCTTTCAACACGCAGGACAG
H-TGF-β1	GGACCAGTGGGGAACACTAC	AGAGTCCCTGCATCTCAGAGT
H-Smad3	GTGCTGGGGTTAGGTCACTG	GAATGTCGCATCCTGTGGGA
H-Smad7	GGAGGTCATGTTCGCTCCTT	GTTTGGTCCTGAACATGCGG
H-α-SMA	GAGGGAAGGTCCTAACAGCC	TAGTCCCGGGGATAGGCAAA
H-Col1	GCTCGTGGAAATGATGGTGC	ACCCTGGGGACCTTCAGAG
H-GAPDH	GAAAGCCTGCCGGTGACTAA	AGGAAAAGCATCACCCGGAG
R-miR-192	RT: CUGCCAGUUCCAUAGGUCACAGGTCGTATCCAGTGCGTGTCGTGGAGTCGG CAATTGCACTGGATACGACCTGTGACC	
	GCGCTGCCAGTTCCATAGG	CAGTGCGTGTCGTGGAGT
R-U6	RT: GTCGTATCCAGTGCAGGGTCCGAGGTATTCGCACTGGATACGACAAAAAT	
	ACGATGCACCTGTACGATCA	TCTTTCAACACGCAGGACAG
R-TGF-β1	GACTCTCCACCTGCAAGACC	GGACTGGCGAGCCTTAGTTT
R-Smad3	CTGGGCAAGTTCTCCAGAGTT	AAGGGCAGGATGGACGACAT
R-Smad7	GAGTCTCGGAGGAAGAGGCT	CTGCTCGCATAAGCTGCTGG
R-α-SMA	CATCACCAACTGGGACGACA	TCCGTTAGCAAGGTCGGATG
R-Col1	GTACATCAGCCCAAACCCCA	CAGGATCGGAACCTTCGCTT
R-GAPDH	AGTGCCAGCCTCGTCTCATA	GGTAACCAGGCGTCCGATAC

H, Human; R, Rat; miR, microRNA; TGF-β1, transforming growth factor-β1; α-SMA, α-smooth muscle actin; col1, collagen type 1; RT, reverse transcription.

performed. Cells were then transferred to PVDF membranes (Thermo Fisher Scientific, Inc.). The PVDF membranes were blocked with 6% non-fat dry milk at 37˚C for 1 h. Immunoblotting was performed using anti-TGF-β1 (1:200; cat. no. ab92486), anti-Smad3 (1:1,000; cat. no. ab40854), anti-Smad7 (1:500; cat. no. ab227309), anti-collagen type 1 (col1; 1:500; cat. no. ab6308), anti-α-smooth muscle actin (anti-α-SMA; 1:1,000; cat. no. ab32575) and anti-GAPDH (1:1,000; cat. no. ab8245) at 37˚C for 2 h, followed by incubation with anti-rabbit/mouse horseradish peroxidase-conjugated IgG secondary antibodies (1:5,000; cat. nos. ab6721 and ab190475, respectively) at 37˚C for 1 h. All antibodies were from Abcam. Antibody incubation was followed the detection of immunoblots and visualization using enhanced chemiluminescence Western Blotting Substrate (Pierce; Thermo Fisher Scientific, Inc.; cat. no. 32106). GAPDH levels were used for normalization. Protein bands were scanned and quantified using a ChemiDoc MP Image analysis system (cat. no. 170-8280; Bio-Rad Laboratories, Inc.).

Renal histological examination. The kidney tissues were fixed in 4% (w/v) paraformaldehyde in PBS at room temperature for 20 min and then sliced into 3-μm-thick sections after paraffin embedding. The paraffin sections were deparaffinized and rehydrated prior to staining with hematoxylin and eosin (H&E) (room temperature; 20 min) for the examination of kidney cellular structure and with Masson's trichrome stain (room temperature; 10 min) for the detection of collagen deposition in the renal interstitium. Visual analysis was performed using an Olympus inverted microscope (magnification, x400; cat. no. CX71; Olympus Corporation

Immunohistochemistry. The aforementioned 3-μm-thick kidney tissue sections were stained immunohistochemically with antibodies against TGF-β1 (1:1,000; cat. no. ab92486, Abcam), Smad3 (1:500; cat. no. ab40845; Abcam) and α-SMA (1:500; cat. no. bs-10196R; BIOSS). After deparaffin (xylene and gradient ethanol) and rehydration, slices were boiled for 15 min using microwave irradiation for antigen retrieval in citrate buffer (0.01 mol/l; pH 6.0). Slices were then washed three times with PBS and blocked with 5% bovine serum albumin (Gibco; Thermo Fisher Scientific, Inc.) for 30 min at room temperature. The slides were incubated with the aforementioned primary antibodies for 2 h at room temperature. Goat anti-rabbit IgG peroxidase conjugate (1:500; cat. no. bs-0295G, BIOSS) was used as the secondary antibody. Cells were incubated with secondary antibodies for 1 h and room temperature. 3,39-diaminobenzidine, nitro

Table II. Blood glucose, body weight, KW/BW, urine protein, creatinine and blood urea nitrogen after ASI treatment for 8 weeks (n=6).

Group	Sham	Model	Model + ASI
Body weight (g)	326.97±18.83	212.33±13.74[a]	283.22±13.65[b]
Blood glucose (mg/dl)	103.1±6.06	315.85±12.17[a]	225.86±20.33[b]
KW/BW (mg/g)	8.13±0.47	13.47±1.36[a]	9.93±0.98[b]
Urine protein (mg)	11.83±1.99	62.32±4.54[a]	33.37±2.57[b]
Creatinine (μmol/l)	34.38±2.88	90.73±3.69[a]	56.95±4.73[b]
Blood urea nitrogen (mmol/l)	10.07±2.34	28.56±1.70[a]	21.37±2.92[b]

Data are presented as the mean ± standard deviation. [a]P<0.05 vs. sham group; [b]P<0.05 vs. model group. ASI, ASI, astragaloside IV; KW, kidney weight; BW, body weight.

blue tetrazolium and 5-bromo-4-chloro-3-indolyl phosphate (all, Sigma-Aldrich; Merck KGaA) were used as enzyme substrates. Finally, after dehydration with gradient ethanol and permeabilization with xylene, the slides were sealed and photographed. Visual analysis was performed using an Olympus inverted light microscope (magnification, x400; cat. no. CX71; Olympus Corporation). The mean optical density (MOD) was calculated using Image Pro Plus 6.0 software (Media Cybernetics, Inc.).

Statistical analysis. Data were analyzed and graphed using GraphPad Prism 5 (GraphPad Software, Inc.). All results are presented as the mean ± standard deviation. Statistically significant differences between groups were determined using a Student's t-test. Multiple comparisons were made among three or more groups using one-way ANOVA followed by the Bonferroni post-hoc test. The nonparametric Mann-Whitney U test was used if data were not normally distributed. P<0.05 was considered to indicate a statistically significant difference.

Results

ASI downregulates the expression of miR-192, which is induced by HG in vitro. Compared with the LG group, miR-192 expression in RMCs was significantly upregulated in the HG group (Fig. 1A). Furthermore, low concentration (10 g/ml) of ASI exhibited no significant effect on miR-192 expression, the greater the ASI concentration, the more obvious the effect. The results revealed that ASI downregulated miR-192 expression in a dose-dependent manner (Fig. 1B). These results demonstrated that HG upregulated and ASI downregulated miR-192 expression *in vitro*.

ASI inhibits HG-induced excessive proliferation in RMCs. The results of the cell proliferation assay revealed that the OD values of the HG group were significantly higher compared with those in the LG group at 72 h (Fig. 1C), which indicated that HG increased the excessive proliferation of RMCs. Treatment with ASI decreased the OD values in a dose-dependent manner compared with untreated cells (Fig. 1D). These results indicated that ASI inhibited the HG-induced excessive proliferation of RMCs in a dose-dependent manner.

ASI alleviates HG-induced fibrosis in RMCs. Using RT-qPCR and western blot analysis, TGF-β1, Smad3, col1 and α-SMA mRNA and protein expression was revealed to be significantly increased and Smad7 mRNA and protein expression was decreased in the HG group compared with the LG group. After ASI treatment, the mRNA and protein levels of TGF-β1, Smad3, col1, and α-SMA were significantly decreased and those of Smad7 were increased in the HG + ASI group compared with the HG group (Fig. 2). These results indicated that ASI alleviated HG-induced fibrosis in RMCs.

ASI exhibits therapeutic effects on DN injury. The model group exhibited a significantly lower weight and elevated blood glucose levels compared with the sham group, and ASI treatment was demonstrated to alleviate weight loss and reduce blood glucose levels (Table II). Furthermore, relative kidney weight was significantly increased in the model group compared with the sham group, whereas ASI treatment led to a significant reduction in kidney weight/body weight ratio compared with the model group (Table II). The results of biochemical analysis demonstrated that urine protein, creatinine and blood urea nitrogen levels in the model group were significantly higher compared with the sham group, and were reduced after ASI treatment (Table II).

In the renal histological examination, H&E staining revealed basement membrane thinning (blue arrows), glomerular atrophy (yellow arrows) and proximal convoluted tubule damage (green arrows) in the model group, and these pathological structures were improved after ASI treatment (Fig. 3). Masson staining revealed interstitial fibrosis and glomerular sclerosis (blue areas) in the model group, and a reduction in interstitial fibrosis after ASI treatment (Fig. 3). These comparisons indicated that ASI exhibited therapeutic effects on DN-induced cell injury.

ASI exhibits therapeutic effects on renal fibrosis in mice. As presented in Fig. 4, the miR-192 expression levels and mRNA and protein expression levels of TGF-β1, Smad3, col1 and α-SMA were significantly increased, and those of Smad7 were decreased, in the model group compared with the sham group. After ASI treatment, the miR-192 expression levels and mRNA and protein expression levels of TGF-β1, Smad3, col1 and α-SMA were significantly decreased and those of Smad7

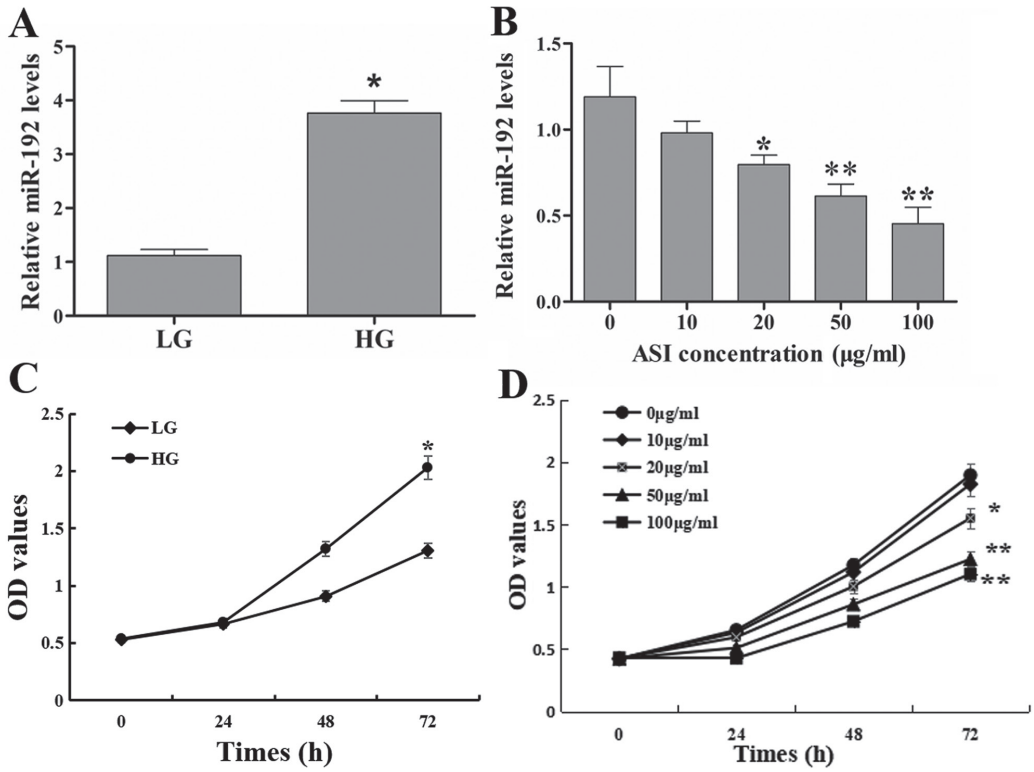

Figure 1. Effects of ASI on miR-192 expression and RMC proliferation. (A) miR-192 expression exhibited by the LG and HG treatment groups. *P<0.05 vs. the LG group. (B) miR-192 expression following treatment with ASI at 0, 10, 20, 50, and 100 μg/ml. *P<0.05 vs. 0 μg/ml ASI group and **P<0.01 vs. 0 μg/ml ASI group. (C) Cell proliferation following treatment with LG and HG. *P<0.05 vs. the LG group. (D) Cell proliferation following treatment with ASI at 0, 10, 20, 50, and 100 μg/ml at 0, 24, 48 and 72 h. *P<0.05 vs. 0 μg/ml ASI group and **P<0.01 vs. 0 μg/ml ASI group. Data are presented as the mean ± standard deviation (n=3). Each bar represents the mean of three independent experiments, and experiments were performed in triplicate. ASI, astragaloside IV; miR, microRNA; RMC, rat mesangial cells; LG, low glucose; HG, high glucose; OD, optical density.

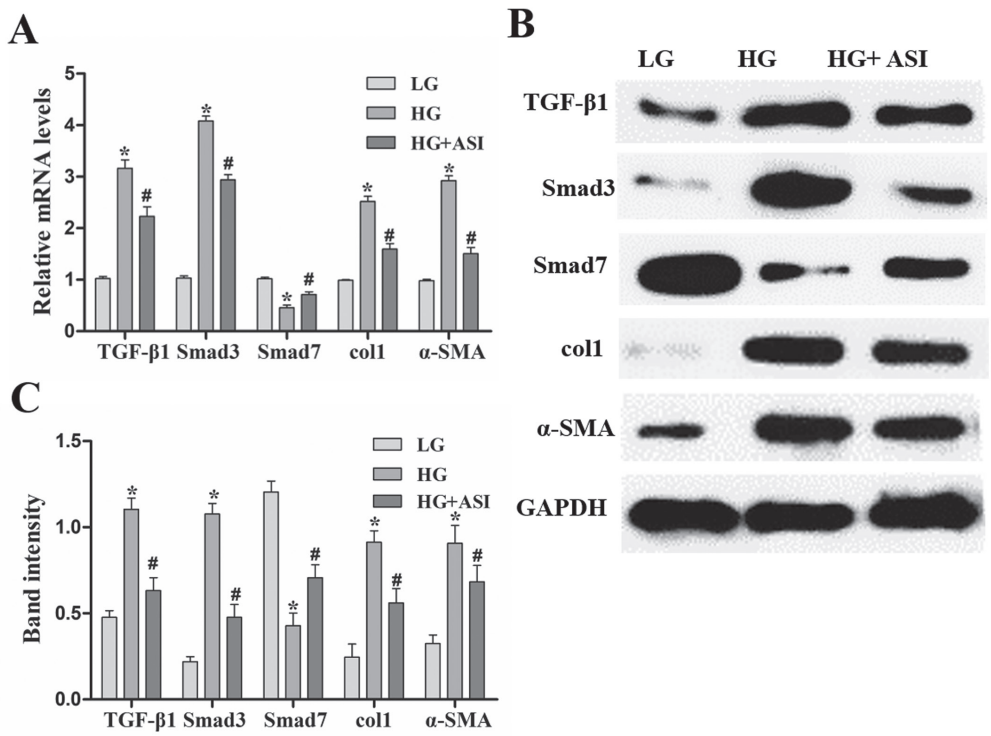

Figure 2. Effects of ASI on the TGF-β1/Smad signaling pathway in RMCs. (A) Reverse transcription-quantitative PCR analysis of TGF-β1, Smad3, col1, α-SMA and Smad7 mRNA in LG, HG and HG + ASI groups. (B) Western blot and (C) subsequent quantification and analysis of TGF-β1, Smad3, col1, α-SMA and Smad7 mRNA in LG, HG and HG + ASI groups. Data are presented as the mean ± standard deviation (n=3). Each bar represents the mean of three independent experiments, and experiments were performed in triplicate. *P<0.05 vs. LG group; #P<0.05 vs. HG group. ASI, astragaloside IV; TGF-β1, transforming growth factor-β1; RMC, rat mesangial cells; col1, collagen type 1; α-SMA, α-smooth muscle actin; HG, high glucose.

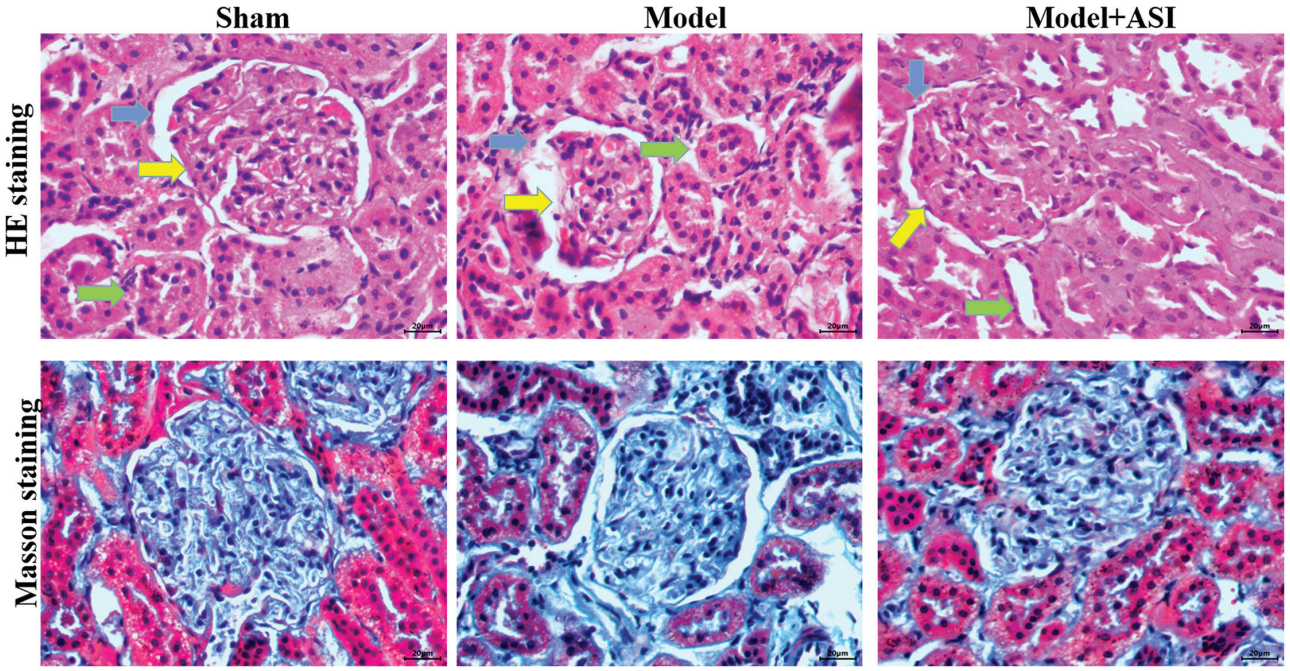

Figure 3. Effects of ASI on in diabetic nephropathy injury. H&E and mason staining of cells in the sham, model and model + ASI groups. magnification, x400. ASI, astragaloside IV; H&E, hematoxylin and eosin. blue arrows, basement membrane; yellow arrows, glomerular atrophy; green arrows, proximal convoluted tubule.

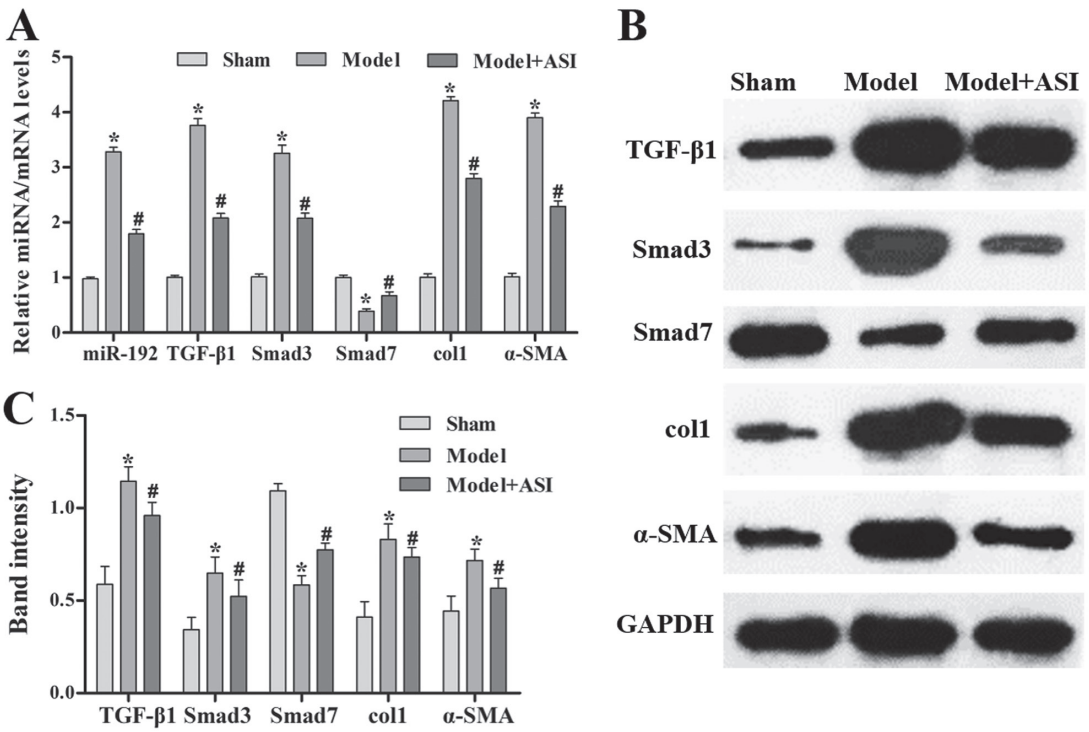

Figure 4. Effects of ASI on the TGF-β1/Smad/miR-192 signaling pathway in rat models of diabetic neuropathy. (A) Reverse transcription-quantitative PCR analysis of relative miR-192, TGF-β1, Smad3, col1, α-SMA and Smad7 expression levels in the sham, model and model + ASI groups. (B) Western blot and (C) subsequent quantification and analysis of TGF-β1, Smad3, col1, α-SMA and Smad7 protein levels in the sham, model and model + ASI groups. Data are presented as the mean ± standard deviation (n=6). *P<0.05 vs. sham group; #P<0.05 vs. model group. ASI, astragaloside IV; TGF-β1, transforming growth factor-β1; miR, microRNA; col1, collagen type 1; α-SMA, α-smooth muscle actin.

were increased in the model + ASI group compared with the model group. Additionally, immunohistochemical assays of TGF-β1, Smad3 and α-SMA supported these previous results (Fig. 5). These results indicated that ASI alleviated renal fibrosis in DN model rats.

Discussion

Radix Astragali has been used as a medicine in China for >2,000 years, and its pharmacological effects and underlying mechanisms are being extensively studied (20). A variety of

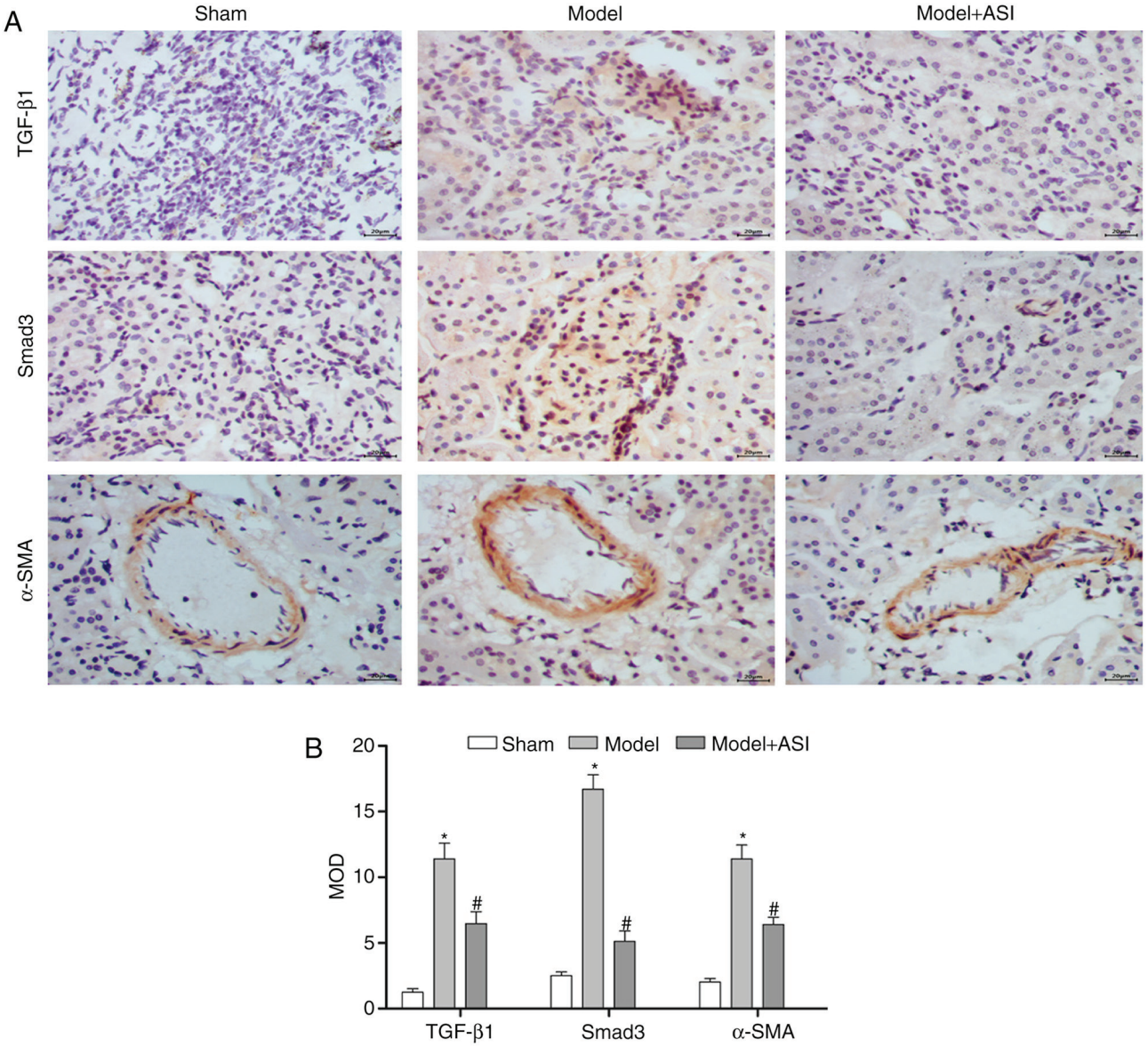

Figure 5. Effects of ASI on the expression of TGF-β1, Smad3 and α-SMA in diabetic nephropathy model rats. (A) Immunohistochemical staining of kidney sections for TGF-β1, Smad3 and α-SMA. (B) The MOD of TGF-β1, Smad3 and α-SMA. The data are presented as the mean ± standard deviation (n=6). *P<0.05 vs. sham group; #P<0.05 vs. model group. Each bar represents the mean of three independent experiments, and experiments were performed in triplicate, with 6 rats. ASI, astragaloside IV; TGF-β1, transforming growth factor-β1; α-SMA, α-smooth muscle actin; MOD, mean optical density.

studies have demonstrated that astragalosides, the major active components of Radix Astragali, exhibit diverse pharmacological effects, including anti-inflammatory, antihypertensive, antidiabetic and myocardial protective effects, *in vitro* and *in vivo* (21-23). The streptozotocin-induced diabetic rat model is characterized by hyperinsulinemia, which results in an increase in blood glucose, a marked reduction in body weight and polyuria (7). The current study assessed the *in vitro* and *in vivo* effects of ASI on DN. After ASI treatment for 8 weeks, blood glucose levels, body weight and kidney weight significant increased compared with the untreated model group. Biochemical indexes (urine protein, creatinine and blood urea nitrogen) of kidney function were also improved, and the pathological changes in the kidney were reduced. In summary, the results of the current study indicated that ASI exhibited therapeutic effects on DN.

TGF-β1 is a major profibrotic factor that drives kidney fibrosis and DN development (7). TGF-β1 activates Smad2 and Smad3, which are two critical downstream mediators that are negatively regulated by Smad7, to perform biological activities, including the production of ECM (24). Some studies have demonstrated that blocking the TGF-β1/Smad3 signaling pathway is an effective therapy for DN (7,8). Additionally, it has been established that excessive collagen deposition is a main characteristic of renal fibrosis and TGF-β1 signaling serves an important role in the stimulation of col1 expression (25,26). During DN progression, α-SMA, which is expressed by myofibroblasts, is located in the renal interstitium and is associated with mesangial proliferation (27). The present study indicated that ASI inhibited the excessive proliferation of HG-induced RMCs, decreased TGF-β1, Smad3, col1 and α-SMA mRNA and protein expression and increased Smad7 mRNA and protein expression *in vitro* and *in vivo*. Therefore, it can be concluded that ASI may be used an effective therapy for DN, and its underlying mechanism may involve the inhibition of excessive

proliferation and renal fibrosis via the TGF-β1/Smad signaling pathway.

Previous studies have revealed that miR-192 is associated with the pathogenesis of DN (28,29) and that miR-192 is enriched in mesangial cells, renal tubular epithelial cells and kidney tissues in experimental diabetes (30). Furthermore, Chung *et al* (31) reported that miR-192 is an important mediator of TGF-β1 signaling in renal fibrosis *in vitro,* and is tightly regulated by TGF-β1, via Smad3, during renal fibrosis. Kato *et al* (32) demonstrated that miR-192 regulated the expression of Smad-interacting protein 1 (an important factor in the TGF-β1/Smad signaling pathway). The results of the current study revealed that miR-192 expression was upregulated in HG-induced RMCs and streptozotocin-induced DN model rats and that ASI downregulated miR-192 expression in a dose-dependent manner. This was accompanied by a decrease in DN injury and expression of fibrosis-related protein, including TGF-β1, Smad3, col1 and α-SMA. The results of the present study indicated that ASI regulated renal fibrosis, resulting from DN, via the miR-192 and TGF-β1/Smad signaling pathways.

In conclusion, the present study demonstrated that ASI exhibits therapeutic effects on DN, which are achieved by inhibiting excessive mesangial proliferation and renal fibrosis via the TGF-β1/Smad/miR-192 signaling pathway. In the future, studies should focus on determining the regulatory relationships between miR-192 and the TGF-β1/Smad signaling pathway, and attempt to identify other relevant molecular mechanisms in DN, such as those involved in signaling pathways that mediate anti-inflammatory effects.

Acknowledgements

Not applicable.

Funding

The current study was supported by the Health Technology Innovation Project of Jilin Province (grant no. 2017J076).

Availability of data and materials

The datasets used and/or analyzed during the present study are available from the corresponding author on reasonable request.

Authors' contributions

LL and QM conceived and designed the experiments. CC, XC and QM performed the experiments. HL and SZ performed the statistical analysis. CC and XC wrote the manuscript. All authors gave final approval of the version to be published.

Ethics approval

The experimental studies were approved by The Institutional Animal Care and Use Committee of Guangzhou Youdi Bio-technology Co., Ltd. (approval no. Y20170623).

Patient consent for publication

Not applicable.

Competing interests

The authors declare that they have no competing interests.

References

1. Wild S, Roglic G, Green A, Sicree R and King H: Global prevalence of diabetes: Estimates for the year 2000 and projections for 2030. Diabetes Care 27: 1047-1053, 2004.
2. Coughlan MT, Cooper ME and Forbes JM: Renal microvascular injury in diabetes: RAGE and redox signaling. Antioxid Redox Signl 9: 331-342, 2007.
3. Battisti WP, Palmisano J and Keane WE: Dyslipidemia in patients with type 2 diabetes. Relationships between lipids, kidney disease and cardiovascular disease. Clin Chem Lab Med 41: 1174-1181, 2003.
4. Bergrem H and Leivestad T: Diabetic nephropathy and end-stage renal failure: The Norwegian story. Adv Ren Replace Ther 8: 4-12, 2001.
5. Kolset SO, Reinholt FP and Jenssen T: Diabetic nephropathy and extracellular matrix. J Histochem Cytochem 60: 976-986, 2012.
6. Yu R, Mao J, Yang Y, Zhang Y, Tian Y and Zhu J: Protective effects of calcitriol on diabetic nephropathy are mediated by down regulation of TGF-β1 and CIP4 in diabetic nephropathy rat. Int J Clin Exp Pathol 8 3503-3512, 2015.
7. Al-Rasheed NM, Al-Rasheed NM, Al-Amin MA, Hasan IH, Al-Ajmi HN, Mohammad RN and Attia HA: Fenofibrate attenuates diabetic nephropathy in experimental diabetic rat's model via suppression of augmented TGF-β1/Smad3 Signaling pathway. Arch Physiol Biochem 122: 186-194, 2016.
8. Sato M, Muragaki Y, Saika S, Roberts AB and Ooshima A: Targeted disruption of TGF-beta1/Smad3 signaling protects against renal tubulointerstitial fibrosis induced by unilateral ureteral obstruction. J Clin Invest 112: 1486-1494, 2003.
9. State Pharmacopoeia Commission. Pharmacopoeia of the People's Republic of China. 2005 edition. Beijing, Chemical Industry Press, 2005: 212-212, 2005.
10. Wu HW, Fang J, Tang LY, Lu P, Xu H, Zhao Y, Li D, Zhang Y, Fu M and Yang H: Quality evaluation of Astragali radix based on DPPH radical scavenging activity and chemical analysis. Chin Herbal Med 6: 282-289, 2014.
11. He JX, Mou QQ, Zhang JQ, Tian Q, He C, Yin R and Li H: Rapid identification of Astragali radix from different origins by UPLC combined with chemometrics methods. Chin Traditional Herbal Drugs 48: 179-184, 2017.
12. Yan MM, Wei L, Fu YJ, Zu YG, Chen CY and Luo M: Optimisation of the microwave-assisted extraction process for four main astragalosides in radix Astragali. Food Chem 119: 1663-1670, 2010.
13. Ren S, Zhang H, Mu Y, Sun M and Liu P: Pharmacological effects of Astragaloside IV: A literature review. J Tradit Chin Med 33: 413-416, 2013.
14. Zhang WD, Chen H, Zhang C, Liu RH, Li HL and Chen HZ: Astragaloside IV from *Astragalus membranaceus* shows cardioprotection during myocardial ischemia in vivo and in vitro. Planta Med 72: 4-8, 2006.
15. Liu H, Wei W, Sun WY and Li X: Protective effects of astragaloside IV on porcine-serum-induced hepatic fibrosis in rats and in vitro effects on hepatic stellate cells. J Ethnopharmacol 122: 502-508, 2009.
16. Yuan X, Gong Z, Wang B, Guo X, Yang L, Li D and Zhang Y: Astragaloside inhibits hepatic fibrosis by modulation of TGF-β1/Smad signaling pathway. Evid Based Complement Alternat Med 2018: 3231647, 2018.
17. Ye J, Coulouris G, Zaretskaya I, Cutcutache I, Rozen S and Madden T: Primer-BLAST: A tool to design target-specific primers for polymerase chain reaction. BMC Bioinformatics 13: 134, 2012.
18. Livak KJ and Schmittgen TD: Analysis of relative gene expression data using real-time quantitative PCR and the 2(-Delta Delta C(T)) method. Methods 25: 402-408, 2001.
19. Shivananjappa MM and Muralidhara: Abrogation of maternal and fetal oxidative stress in the streptozotocin-induced diabetic rat by dietary supplements of Tinospora cordifolia. Nutrition 28: 581-587, 2012.
20. Sun XY and Sun FY: Shen Nong Ben Cao Jing. Taiyuan, Shanxi Science and Technology Press, pp112-113, 2010.

21. He Y, Du M, Gao Y, Liu H, Wang H, Wu X and Wang Z: Astragaloside IV Attenuates experimental autoimmune encephalomyelitis of mice by counteracting oxidative stress at multiple levels. PLoS One 8: e76495, 2013.
22. Wang ZS, Xiong F, Xie XH, Chen D, Pan JH and Cheng L: Astragaloside IV attenuates proteinuria in streptozotocin-induced diabetic nephropathy via the inhibition of endoplasmic reticulum stress. BMC Nephrol 16: 44, 2015.
23. Zhang N, Wang XH, Mao SL and Zhao F: Astragaloside IV improves metabolic syndrome and endothelium dysfunction in Fructose-fed rats. Molecules 16: 3896-3907, 2011.
24. Wang D, Zhang G, Chen X, Wei T, Liu C, Chen C, Gong Y and Wei Q: Sitagliptin ameliorates diabetic nephropathy by blocking TGF-β1/Smad signaling pathway. Int J Mol Med 41: 2784-2792, 2018.
25. Kalluri R and Neilson EG: Epithelial-mesenchymal transition and its implications for fibrosis. J Clin Invest 112: 1776-1784, 2003.
26. Izumi N, Mizuguchi S, Inagaki Y, Saika S, Kawada N, Nakajima Y, Inoue K, Suehiro S, Friedman SL and Ikeda K: BMP-7 opposes TGF-beta 1-mediated collagen induction in mouse pulmonary myofibroblasts through Id2. Am J Physiol Lung Cell Mol Physiol 290: L120-L126, 2006.
27. Li J, Qu X and Bertram JF: Endothelial-myofibroblast transition contributes to the early development of diabetic renal interstitial fibrosis in streptozotocin-induced diabetic mice. Am J Pathol 175: 1380-1388, 2009.
28. Ma X, Lu C, Lv C, Wu C and Wang Q: The expression of miR-192 and its significance in diabetic nephropathy patients with different urine albumin creatinine ratio. J Diabetes Res 2016: 6789402, 2016.
29. Liu F, Zhang ZP, Xin GD, Guo LH, Jiang Q and Wang ZX: miR-192 prevents renal tubulointerstitial fibrosis in diabetic nephropathy by targeting Egr1. Eur Rev Med Pharmacol Sci 22: 4252-4260, 2018.
30. Wang B, Herman-Edelstein M, Koh P, Burns W, Jandeleit-Dahm K, Watson A, Saleem M, Goodall GJ, Twigg SM, Cooper ME and Kantharidis P: E-cadherin expression is regulated by miR-192/215 by a mechanism that is independent of the profibrotic effects of transforming growth factor-beta. Diabetes 59: 1794-1802, 2010.
31. Chung AC, Huang XR, Meng X and Lan HY: miR-192 mediates TGF-beta/Smad3-driven renal fibrosis. J Am Soc Nephrol 21: 1317-1325, 2010.
32. Kato M, Zhang J, Wang M, Lanting L, Yuan H, Rossi JJ and Natarajan R: MicroRNA-192 in diabetic kidney glomeruli and its function in TGF-beta-induced collagen expression via inhibition of E-box repressors. Proc Natl Acad Sci USA 104: 3432-3437, 2007.